

# Computational Analysis of Blood Flow in Human Aorta

Ali C. Benim<sup>1</sup>, Fethi Gul<sup>1</sup>, Ali Nahavandi<sup>1</sup>, Alexander Assmann<sup>2</sup>,  
Peter Feindt<sup>3</sup> and Franz Joos<sup>4</sup>

<sup>1</sup>Department of Mechanical and Process Engineering, Duesseldorf University of Applied Sciences, Josef-Gockeln-Str. 9, D-40474 Duesseldorf, Germany,  
E-mails: alicemal.benim@fh-duesseldorf.de, ali.nahavandi@fh-duesseldorf.de, fethi.guel@fh-duesseldorf.de

<sup>2</sup>Department of Cardiovascular Surgery, University Hospital, Moorenstr. 5, D-40225 Duesseldorf, Germany, E-mails: alexander.assmann@med.uni-duesseldorf.de

<sup>3</sup>Department of Thoracic Surgery, Clemenshospital, Muenster, Germany  
E-mail: p.feindt@clemenshospital.de

<sup>4</sup>Laboratory of Turbomachinery, Helmut Schmidt University, Holstenhofweg 85, D-22043 Hamburg Germany, E-mail: joos@hsu-hh.de

## ABSTRACT

Extracorporeal circulation is a method in cardiovascular surgery that can be used in different variations. Computational fluid dynamics can be applied to predict the impact of a certain technique for a patient preoperatively, by taking the patient-specific physiology into account. By the developed methodology, the aortic geometry of a patient can be captured and analyzed. In the present work, the physiological blood flow, as well as the antegrade extracorporeal circulation are computationally investigated for a patient with an anomaly in the aortic physiology. The same flow configurations are investigated for an idealized aorta. The results are compared. It is shown that the consequences of the antegrade extracorporeal circulation for an abnormal and idealized/normal aorta turn out to be different. This comparison indicates that it is commendable to perform a patient-specific detailed computational analysis in advance, for the patients with abnormal physiology, instead of assuming a normal behavior for extracorporeal circulation.

## 1. INTRODUCTION

Biofluidynamics is a new and rapidly expanding field of science that combines engineering with medical research [1]. Even though various biological flows, like the air flow in pulmonary system [2] are being considered, the blood flow dynamics stays quite in the foreground [3]. This is also the subject of the present investigation. In particular, blood flow in human aorta is of present interest, with emphasis on antegrade extracorporeal circulation [4].

In the field of artificial heart valves and circulatory assist devices, one can look back at a rather large amount of studies [5, 6]. However, a comparably small number of investigations concentrate on the details of the aortic blood flow, especially in the context of extracorporeal circulation. Wood et al. [7] presented a comparison of the aortic magnetic resonance imaging data with the predictions of a numerical simulation. Lee and Chen [8] performed a numerical investigation with emphasis on the prediction of physiological wall shear stress and blood flow profiles in the abdominal aorta. To the opinion of present authors, there is still a lack in numerical and experimental investigations for the influence of extracorporeal circulation on the aortic flow field.

As far as the extracorporeal circulation is concerned, Tokuda et al. [9] performed a numerical simulation of the antegrade perfusion of the ascending aorta during cardiopulmonary bypass, using the finite element method. They predicted “turbulences” in the aortic arch that play an important role in the delamination and sequential embolization of arteriosclerotic plaques.

Nevertheless, even though they referred to the phenomena of “turbulence”, they did not give any information about, if any or which turbulence model was applied. Minakawa et al. [10] performed an experimental investigation of retrograde perfusion via the axillary artery. Using particle image velocimetry, they detected quite high flow velocities and turbulence intensities in the ascending aorta, respectively the aortic arch.

To the best of the authors’ knowledge, a comparative analysis of extracorporeal circulation on the

aortic flow patterns, and especially on the aortic wall shear stress distributions has not yet been performed, except for a recent investigation of the present authors [11], where both antegrade and retrograde perfusion techniques for extracorporeal circulation were numerically analyzed and compared for an idealized aortic geometry. The present investigation is an improvement of that work [11], where, now, the real aortic geometry for an individual patient is captured, represented and analyzed. In the present analysis, pulsatile and steady-state physiological circulation as well as pulsatile and steady-state extracorporeal circulation via antegrade perfusion are investigated. Predictions are performed for two aortic geometries, namely for an idealized aortic geometry and a realistic aorta physiology that exhibits an anomaly: An adult patient, who had to be operated due to coronary artery disease, suffered from a compensated aortic isthmus stenosis that did not cause significant hemodynamical alterations. The results obtained for both geometries are compared with each other. Conclusions are drawn for the application of extracorporeal circulation via antegrade perfusion to abnormal aortic geometries, in comparison to the normal physiological constitution.

## 2. MODELLING

### 2.1 Geometry Capturing, Boundaries, Grid Generation

The starting point for capturing the aortic geometry of a certain patient is the Magnetic Resonance Imaging (MRI) data stored according to DICOM standards [12]. Via open source software 3D Slicer [13] and Bioimage Suite [14], as well as using an in-house developed interface program, the geometry data is imported in Gambit [15], the grid generator of the CFD software Fluent [15]. The “idealized” geometry considered for the “normal” aorta is principally based on the data obtained on a healthy person. In that case, the idealized geometry is directly generated within the grid generator Gambit [15].

For each aortic physiology, two different geometry models are generated: one for simulating the physiological circulation, considering the basic aorta geometry, and one for simulating the extracorporeal circulation applying an antegrade perfusion, by considering the insertion of the cannula into the aorta. In what follows, the idealized aortic geometry will be designated by “A-1”, whereas the realistic aorta geometry of the individual patient exhibiting an anomaly (aortic isthmus stenosis) will be designated by “A-2”.

Geometries A-1 and A-2, for the case of antegrade perfusion (including the inserted cannula) are displayed in Figure 1. Detail views in the near-field of cannula injection are also presented in the figure. For the antegrade perfusion, the blood is injected through the cannula as indicated by arrows in Figure 1. Thus, the inlet boundary of the computational domain is placed at the outlet of the cannula. In Figure 1, the main flow direction is also indicated by arrows. For the physiological circulation, there is no cannula inserted, and the inlet boundary is placed at the upstream end of the aorta. This boundary is positioned at a somewhat downstream position from the heart valve, and is defined to be an impermeable wall for the case of antegrade perfusion (clamped under surgery conditions). In Figure 1, the labeling of the aortic branches is also shown, which will be used in defining boundary conditions.

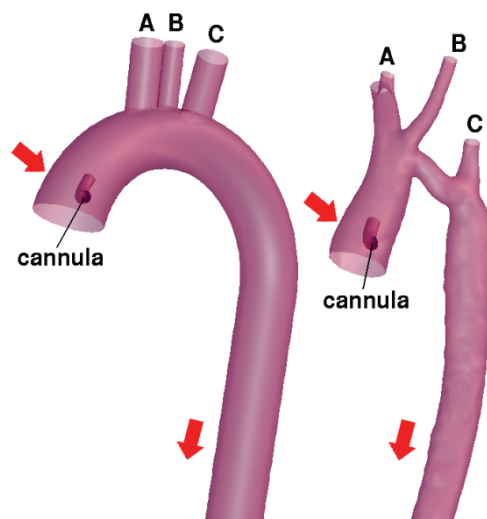


Figure 1. Aortic geometries, left: A.-1, right: A-2.

In grid generation, an unstructured technique is applied, where tetrahedral and hexahedral cells are used in a combined manner. A formal grid independency study, specific to the present case is not performed, relying on the previous experience [11,16] in that respect. Since similar grid resolutions are applied in both cases, and since the present investigation aims a comparison between the two simulations (without any comparison with measurements), we are rather confident that the present approach would lead to meaningful results as far as the comparative assessment of the two cases is concerned. The generated grids that have approximately 350,000 cells are displayed in Figure 2.

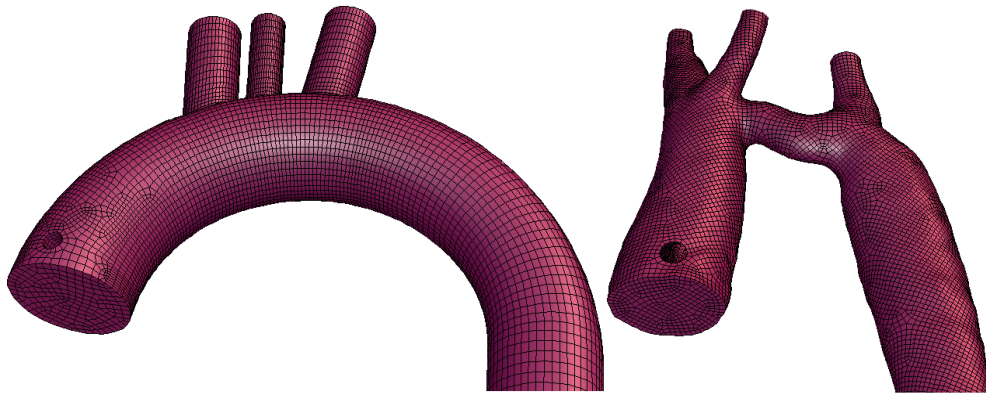


Figure 2. Computational grids, left: A.-1, right: A-2.

## 2.2 Mathematical and Numerical Modelling

Three-dimensional, steady-state, incompressible and unsteady (pulsatile) flows are investigated. The wall deformability is neglected. In large arteries, such as the aorta, shear stresses are normally sufficiently large to assume a Newtonian behaviour of the blood [17]. Thus, a Newtonian behaviour is assumed for the blood, in the present study, for present purposes. Thus, Navier-Stokes equations with constant material properties are solved.

Depending on the geometry and the mode of circulation, the local and temporal Reynolds numbers vary around values that can be assumed to be critical for laminar-to-turbulent transition., calling for an adequate turbulence modelling approach. For the physiological circulation, the Reynolds number ( $Re$ ) at the inlet of A-1 was about 1150, based on the local diameter and the time-averaged bulk velocity. On the other hand, for the antegrade perfusion, the time-averaged inlet Reynolds number ( $Re$  at the cannula outlet) was much higher, i.e. about 6000. It is known that the laminar-to-turbulence transition typically occurs around the critical value of  $Re = 2300$ , for a pipe flow (whereby it is also known that this critical value has a rather indicative role, and transition to turbulence may occur at different values of  $Re$ , depending on flow conditions). Thus, one can assume that transitional effects can play a role in the flow under consideration. Based on the temporally minimum inlet velocities, a rather laminar flow throughout the aorta may rather be expected for the physiological flow (although local effects causing local turbulence generation in the downstream may not be precluded a priori). However, the peak inlet velocities during a pulse temporally cause sufficiently high inlet Reynolds numbers (around 5000-6000) to temporally onset turbulence during a pulse. For the antegrade perfusion, the inlet  $Re$  indicates a turbulent flow in both circulation modes (for the steady-state operation or pulsatile operation of the heart-lung machine), which, but, may re-laminarize in the downstream. Transition modelling is still a difficult area in turbulence modelling, especially in unsteady cases like the present one. Nevertheless, for optimally coping with the situation, based on the available modelling capabilities, the flow was modelled as turbulent via the so-called “Shear Stress Transport” model [18], which is a two-equation model that can “principally” accommodate for some transitional effects.

The differential transport equations are discretized by a co-located Finite Volume Method. For handling the velocity-pressure coupling, the SIMPLEC and PISO algorithms are used in steady-state and pulsatile computations, respectively. For discretizing the convective terms, the Power-Law scheme is used [19]. In the pulsatile computations, a second-order implicit time discretization is used [19]. Time-step sizes are determined in such a manner that the maximum cell Courant numbers [19] remain

below unity. In the pulsatile simulations, the flow is computed, first, for a period of several pulses, until a fully periodic flow pattern is achieved. Thereafter, the time-averaging is performed. Thus, an eventual influence of the rather arbitrary initial conditions on the unsteady results and on their time-average is prevented.

### 2.3 Boundary Conditions

For the physiological circulation, the inlet boundary is placed nearly at the position of the heart valve (slightly downstream of the latter). For the antegrade perfusion, the inlet boundary is positioned to be at the geometric outlet of the cannula. The upstream part of the aorta is also shortened slightly, for taking into account that the aorta is clamped just downstream the heart valve during surgery. In that case, the upstream boundary of the aorta (corresponding to the inlet boundary of the physiological circulation) is declared to be a wall. At inlets, for all cases, spatially uniform distributions are prescribed for all variables, assuming the velocity being normal to the boundary, and the inlet boundary conditions of the turbulence quantities are derived assuming a local turbulence intensity and a length scale. For the turbulence intensity, rather low values are prescribed (0.1%) if the inlet Reynolds number is indicating a theoretically laminar flow. Otherwise, a turbulence intensity of 4% is prescribed. The macro length scale is always assumed to be 30% of the inlet (hydraulic) diameter.

For the pulsatile simulation of the physiological circulation, the pulse shape reported in [20] at a further downstream position of the aortic valve (at the position of the carotid artery) is assumed, which is slightly different from the one reported [19] at the heart valve position. In doing this, it is assumed that the shift in the pulse shapes between the two positions is majorly caused by the deformability of the aortic walls, as such effects are known to play a role especially in the initial regions of the aorta. Since the wall deformability is not modelled in the present investigation, this pulse shape [20] is assumed to be more relevant for the present modelling of the flow in the complete aortic domain.

In defining the computational domain, the aortic branches need to be cut at one position, resulting in “outlet” boundaries that need an adequate formulation. It is clear that such boundary conditions cannot readily be formulated. However, it is also obvious that their convenient formulation is very important for the flow distribution between the different branches, thus for the predicted supply of important organs. For the physiological circulation, some empirical values can be assumed for a “normal” distribution between the branches [21]. For example, for the physiological circulation, the percentage distribution provided in Table I can quite reliably be assumed for the branches displayed in Figure 1.

However, for anatomies remarkably deviating from the “normal” one, and for different perfusion techniques applied in extracorporeal circulation, it is difficult to presume that this distribution (Table I) remains to be valid. An alternative approach could be the prescription of the static pressure at outlets (the same value at all outlets). Nevertheless, as already discussed in the previous work [11,22], this boundary definition, although it may work fairly well in some cases, is not reliable, in general. As a further alternative, an outlet boundary condition based on loss-coefficients was formulated by present authors [11,22]. This boundary condition will mainly be used in the present study, by also making comparisons with the alternative formulations. However, for the present study, the flow rate distribution displayed in Table I will be used in all computations, for simplicity, since it has previously been demonstrated that the different formulations do not cause a considerable difference in the present case [23].

Table 1. Distribution of the inlet flow rate among the branches A, B, C (Fig. 1)

Branch	A	B	C
% flow rate	15.0	7.5	7.5

## 3. RESULTS

### 3.1 Pulsatile vs. Steady-State Flow

In this section the physiological circulation in aorta A-2 is considered only, for comparing the steady-state and pulsatile modelling. For the physiological circulation, the steady-state modelling does not have a physical significance. However, it is still considered for comparison purposes. For the physiological circulation in A-2, the predicted contours of time-averaged dimensionless speed (all results are non-dimensionalized by the time-averaged inlet speed) are displayed in Figure 3 in planes

cutting through the aorta and its branches. In the figure, the steady-state results (Fig. 3a), the time-averaged distribution (Fig. 3b), as well as the instantaneous distribution at the moment corresponding to the maximum inlet pulse speed (Fig. 3c) are displayed.

It can be observed that the steady-state prediction (Fig. 3a) and the time-averaged results of the pulsatile solution (Fig. 3b) are practically identical (maximum values are 6.98 for the former and 6.84 for the latter that differ only about 2%) and the steady-state solution can be considered to reliably represent the time-averaged flow field. Both distributions exhibit a rather narrow high velocity zone just upstream the branch C, which is neighbored by quite large recirculation regions in the entry area of branch C, and especially along the inner boundary of the aortic arch. This is essentially caused by the buckling of the aortic arch after the branches A and B (in comparison to the smooth shape of the “normal” A-1). Further recirculation (or low speed) zones can be observed, such as those in the entry region of branch A, or in the descending aorta. In general, a quite unfavourable steady-state (Fig. 3a) or time-averaged (Fig. 3b) velocity distribution is observed for A-2. Although steady-state and time-averaged results are similar, it is obvious that the steady-state (or the time-averaged) solution cannot represent the instantaneous distribution. Looking at the instantaneous dimensionless distribution of the flow speed displayed in Figure 3c at the moment corresponding to the maximum inlet velocity, one can see that much higher values for the non-dimensional speed (maximum value about 31) and stronger inhomogeneities occur.

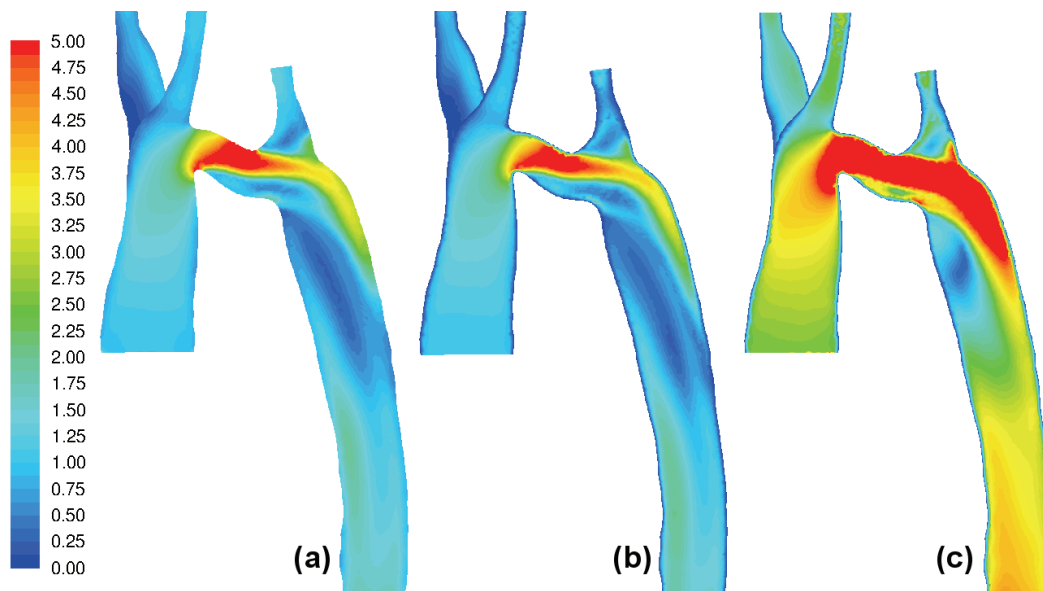


Figure 3. Dimensionless speed distribution for physiological circulation in A-2 (a) steady-state, (b) pulsatile, time-averaged , (c) pulsatile, instantaneous at peak inlet speed.

### 3.2 Physiological Circulation

For the physiological circulation, the predicted distributions of speed in planes cutting through the aorta and branches are illustrated in Figure 4, for A-1 and A-2. The time-averaged distributions are shown in Figure 4a (A-1) and Figure 4b (A-2). Figure 4c (A-1) and Figure 4d (A-2) display the instantaneous distributions at the moment of peak inlet velocity (the maximum speed values in m/s are: 0.45 for Fig. 4a, 1.97 for Fig 4b, 1.11 for Fig. 4c, 4.77 for Fig 4d).

Since A-2 has a smaller inlet, with the same flow rate, the inlet speed of A-2 is higher (about 50%) than that of A-1. One can see that the speed distribution remains rather homogeneous for A-1 for time-averaged (Fig. 4a) and instantaneous (peak inlet speed) distributions (Fig. 4c). A quite inhomogeneous distribution is obtained for A-2, especially for the instantaneous distribution at peak inlet speed (Fig. 4d). Inhomogeneities are observed especially in the region between branches B and C, where, much higher velocity values are attained for A-2 in comparison to A-1, both for the time-averaged and instantaneous fields (Fig. 4).

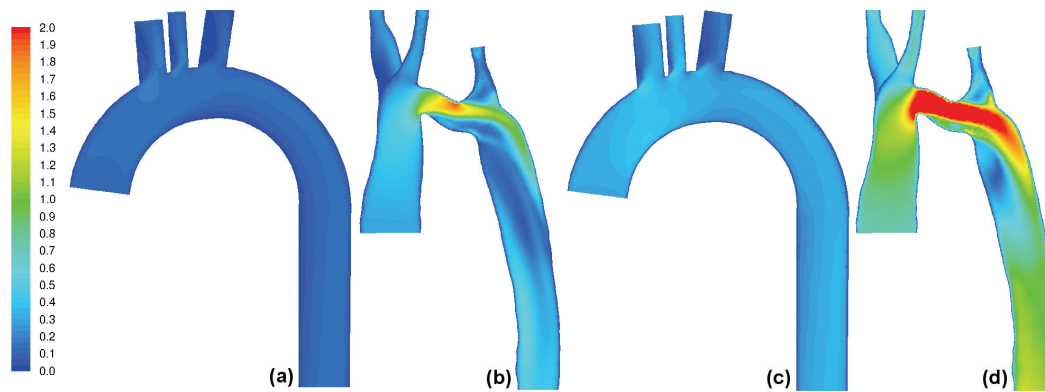


Figure 4. Speed (m/s) distribution for physiological circulation, (a) time-averaged A-1, (b) time-averaged A-2, (c) instantaneous at peak inlet speed A-1, (d) instantaneous at peak inlet speed A-2.

Predicted turbulence kinetic energies are displayed in the same planes for A-1 and A-2, in Figure 5 (the maximum turbulence kinetic energy values in  $\text{m}^2/\text{s}^2$  are: 0.005 for Fig. 5a, 0.080 for Fig 5b, 0.028 for Fig. 5c, 0.575 for Fig 5d). At the inlets the turbulence kinetic energies are similarly low, for A-1 and A-2. As the turbulence kinetic energy remains low in downstream, for A-1, a considerable production of turbulence kinetic energy is observed for A-2. The turbulence is mainly generated by the sharp velocity gradients associated with the large recirculation zone caused by the buckled aortic arch in the region between branches B and C. One can see that the turbulence levels in A-1, even for the instantaneous turbulence distribution for peak inlet velocity are much too low compared to A-2. For A-2, the instantaneous turbulence levels depicted in Figure 5d are much higher of course, compared to the time-averaged distribution (Fig. 5b)

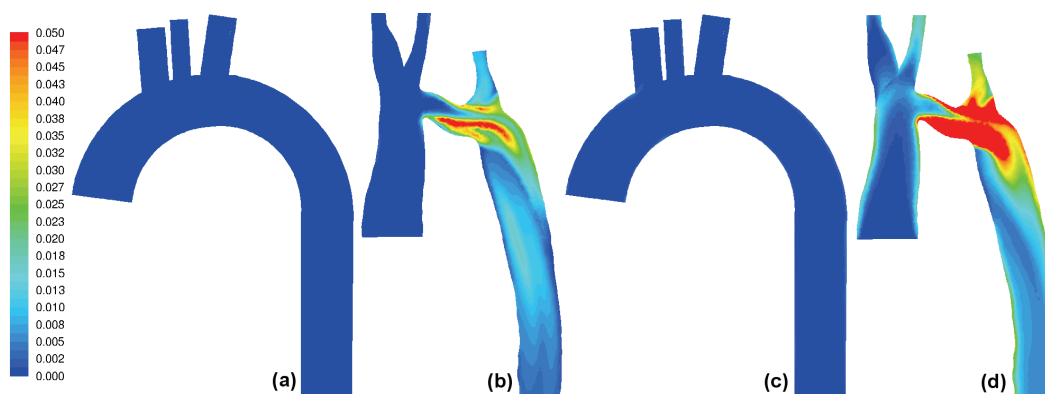


Figure 5. Turbulence kinetic energy ( $\text{m}^2/\text{s}^2$ ) distribution for physiological circulation, (a) time-averaged A-1, (b) time-averaged A-2, (c) instantaneous at peak inlet speed A-1, (d) instantaneous at peak inlet speed A-2.

Figure 6 displays predicted distributions of the wall shear stress for A-1 and A-2 (the maximum wall shear values in Pa are: 6.963 for Fig. 6a, 45.721 for Fig 6b, 27.544 for Fig. 6c, 144.205 for Fig 6d). One can see that very much higher shear stress values are predicted for A-2, compared to A-1. The most critical region is, again, the part of the arch between branches B and C.

### 3.3 Extracorporeal Circulation

In this section, extracorporeal circulation via antegrade perfusion will be investigated. For this case, the time-averaged and the instantaneous distributions of the speed in planes cutting through the aorta and its branches are illustrated in Figure 7, for A-1 and A-2. Please note that the flow rates, in this case, are smaller compared to the physiological circulation (the flow rate of the antegrade perfusion is prescribed to be 80% of that of the physiological circulation). The maximum velocities occur, now, near the inlet

boundary, i.e. either at the outlet of the cannula, or within the jet in the near-field of the cannula, and are quite close to each other for A-1 and A-2, since the same cannula geometry and the same flow rate apply for the both aortic geometries (about 3.5 m/s for the time-averaged distributions, and about 9.0 m/s for the instantaneous fields at the peak inlet velocity). For A-1, much stronger inhomogeneities are observed, now (Fig. 7), in comparison to the physiological circulation (Fig. 3), which are, however, inevitable in this case, of course, due to the jet-like injection of blood through the cannula. For A-2, the inhomogeneities are, however, still stronger. The flow field in the upstream part of A-2, i.e. in the region between the cannula and branches A and B is very complex. In this region, there are comparably strong recirculation zones. This is also the reason, why a high velocity region is observed along the side wall of the initial part of the aorta. This region is associated with a recirculation zone with high near-wall velocities. High velocities are also observed in the part between branches B and C (as it was also the case for physiological circulation, Fig. 4). The inhomogeneities are, of course stronger for the instantaneous distributions (at the peak inlet velocity) compared to the time-averaged distributions (Fig. 7).

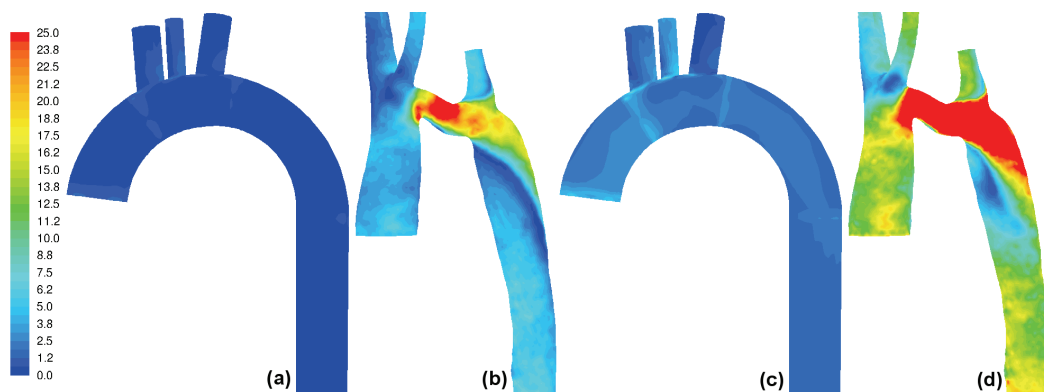


Figure 6. Wall shear stress (Pa) distribution for physiological circulation, (a) time-averaged A-1, (b) time-averaged A-2, (c) instantaneous at peak inlet speed A-1, (d) instantaneous at peak inlet speed A-2.

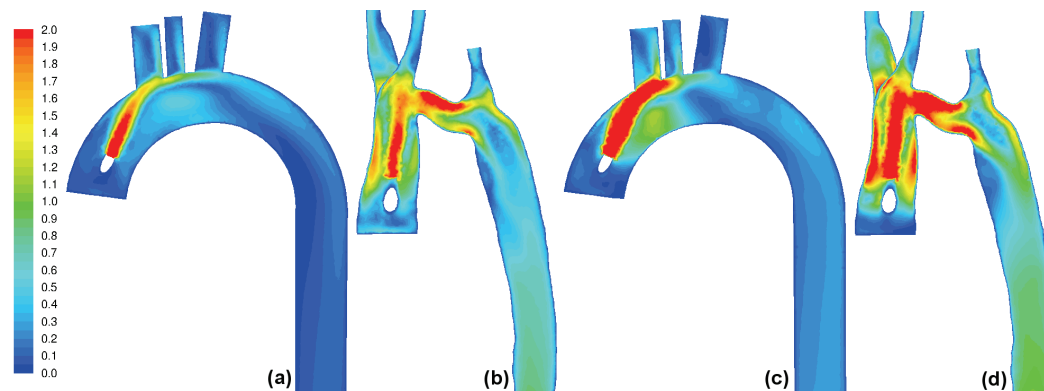


Figure 7. Speed (m/s) distribution for extracorporeal circulation, (a) time-averaged A-1, (b) time-averaged A-2, (c) instantaneous at peak inlet speed A-1, (d) instantaneous at peak inlet speed A-2.

Predicted turbulence kinetic energies are displayed in the same planes for A-1 and A-2, in Figure 8 (the maximum turbulence kinetic energy values in  $m^2/s^2$  are: 0.285 for Fig. 8a, 3.420 for Fig. 8b, 1.886 for Fig. 8c, 3.504 for Fig. 8d). In antegrade perfusion (Fig. 8), the turbulence levels are in general much higher compared to the physiological circulation (Fig. 5), due to the high velocities and turbulence introduced by the cannula jet. The differences in the turbulence levels between A-1 and A-2, in antegrade perfusion (Fig. 8) are also smaller compared to the physiological circulation (Fig. 5), since the flow field of A-1 also exhibits some inhomogeneities compared to the physiological circulation. However, it can still be observed that the turbulence generation is greater in A-2 compared to A-1 (Fig. 8). This is mainly

due to the rather strong recirculation zones in the initial parts, which was already mentioned in association with Figure 7.

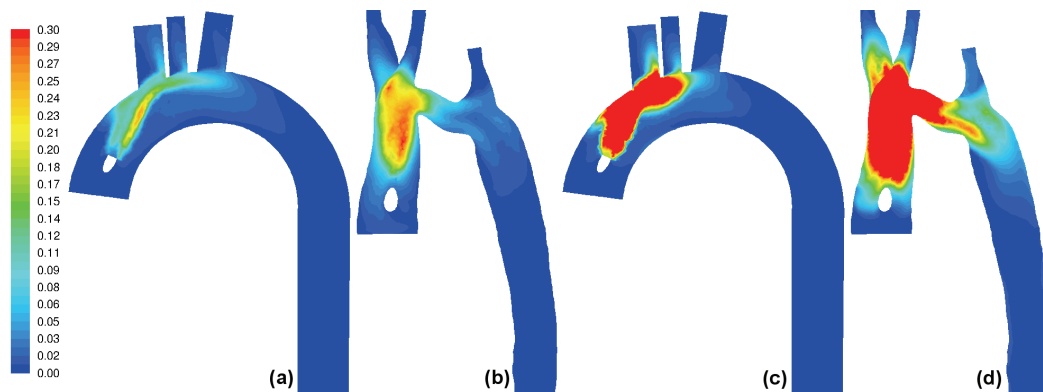


Figure 8. Turbulence kinetic energy ( $\text{m}^2/\text{s}^2$ ) distribution for extracorporeal circulation, (a) time-averaged A-1, (b) time-averaged A-2, (c) instantaneous at peak inlet speed A-1, (d) instantaneous at peak inlet speed A-2.

Figure 9 illustrates the predicted distributions of the wall shear stress for A-1 and A-2 (the maximum wall shear values in Pa are: 43.131 for Fig. 9a, 45.245 for Fig 9b, 92.386 for Fig. 9c, 167.136 for Fig 9d). It is interesting to note that the maximum values predicted for A-2 are similar between physiological circulation (Fig. 6) and antegrade perfusion (Fig. 9). In antegrade perfusion, similar maximum values are also obtained for A-1 and A-2 (Fig. 9). One can also see, however, that the amount of area subject to high wall shear stress is much greater for A-2, compared to A-1 (Fig. 9), which still indicates a much higher risk for A-2 than A-1, due to this reason.

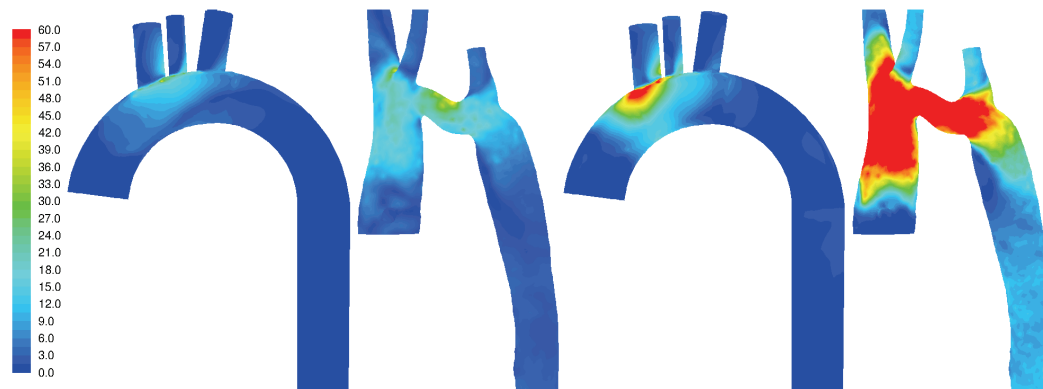


Figure 9. Wall shear stress (Pa) distribution for extracorporeal circulation, (a) time-averaged A-1, (b) time-averaged A-2, (c) instantaneous at peak inlet speed A-1, (d) instantaneous at peak inlet speed A-2.

A comparison of the maximum wall shear stress values for the considered cases is presented in Figure 10. Please note that the presented values are instantaneous values occurring during a pulse period. One can see, again, that the maximum shear stress values for the extracorporeal circulation (EC) are larger than those for the physiological circulation (PC) for both aortic geometries. Nevertheless, the relative increase of the maximum wall shear stress from PC to EC is larger for A-1 compared to A-2. For PC and EC, the maximum walls shear stress values are larger for the aorta with aortic isthmus stenosis (A-2) compared to the idealized aortic geometry (A-1) (Fig. 10).

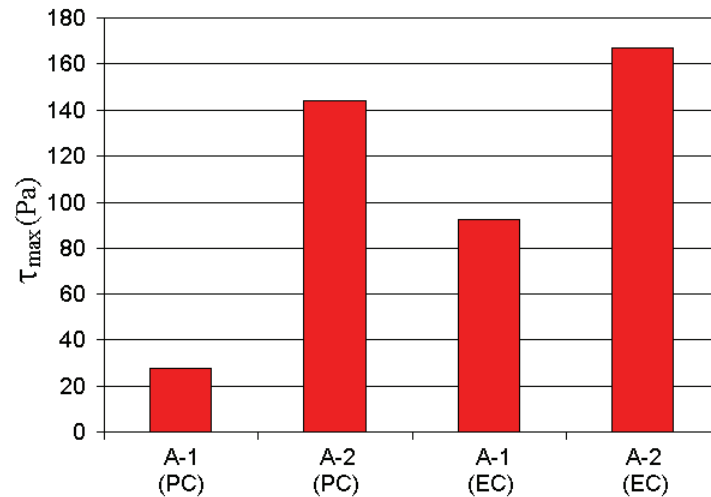


Figure 10. Maximum wall shear stress (Pa) occurring during a pulse period for both aortic geometries A-1 and A-2, during physiological circulation (PC) and extracorporeal circulation (EC).

#### 4. CONCLUSIONS

Based on the present study, the following conclusions can be drawn:

If the time-averaged flow field is of interest, the steady-state predictions can be used, as the both solutions are very similar.

For the physiological circulation, the flow fields of the idealized and abnormal aortas show remarkable differences, where the flow structure observed for the abnormal aorta is quite unfavorable. This holds for both physiological and extracorporeal circulation. Here, an especially critical aspect seems to be the overloading of the region of the aorta between branches B and C.

Subsequently we simulated a scenario in which an adult patient with a mild aortic isthmus stenosis underwent EC for coronary surgery. Numerical analysis revealed, conforming with actual intraoperative observations, that antegrade perfusion of the abdominal aorta via a cannula inserted in the ascending aorta was sufficient. It is demonstrated that the consequences of the extracorporeal circulation for the considered abnormal aorta and the idealized aorta are different. The relative increase of the maximum wall shear stress is larger for the idealized aorta (compared to the abnormal aorta), when the circulation mode changes from physiological to extracorporeal. Still, the maximum shear stress values occurring around the aortic isthmus stenosis are always larger than those occurring in the idealized aorta, both for physiological and extracorporeal circulation. Besides the larger local maximum shear stress values, the sizes of the region of the aortic wall experiencing high wall shear stress are much larger for the abnormal aorta, compared to the idealized aorta. Thus, higher risk of arteriosclerotic plaque mobilization can be assumed for the abnormal aorta, compared to the idealized one. In the extracorporeal circulation, the overloaded region of the aortic wall is not restricted to the region between the branches B and C. High shear stresses are observed also in the very initial parts of the aortic arch due to the high velocities caused by the cannula jet. Moreover, predominantly turbulent flow is observed in the nearfield of the cannulas, as indicated by the increased turbulent kinetic energy levels. Thus, damage of blood elements needs to be considered as a possible consequence.

These comparisons, overall, indicate that the critical flow parameters can change from patient to patient, depending on the individual physiology. Therefore, it is very advisable to perform a patient-specific detailed computational analysis in advance (especially for the patients with abnormal physiology), before surgery, instead of assuming a usual/normal behavior for the extracorporeal circulation.

#### REFERENCES

- [1] J. N. Mazumdar, *Biofluid Mechanics*, World Scientific, Singapore, 1992.
- [2] C. Bertram and D. P. Gaver III, Biofluid mechanics of the pulmonary system, *Annals of Biomedical Engineering*, 33, 2005, 1681-1688.

- [3] G. Pedrizetti and K. Perktold, K. (Eds.), *Cardiovascular Fluid Mechanics*, Springer, Wien, 2003.
- [4] C. T. Mora, R. A. Guyton, D. C. Finlayson and R. L. Rigatti (Eds.), *Cardiopulmonary Bypass: Principles and Techniques of Extracorporeal Circulation*, Springer, Berlin, 1995.
- [5] Y. Yokoyama, D. Medart, M. Hormes, C. Schmitz, K. Hamilton, P. B. Kwant, S. Takatani, T. Schmitz-Rode and U. Steinseifer, CFD simulation of a novel bileaflet mechanical heart valve prosthesis: an estimation of the Venturi passage formed by the leaflets, *International Journal of Artificial Organs*, 29, 2006, 1132-1139.
- [6] H.-D. Li and W. K. Chan, Inverse design and CFD investigation of blood pump impeller, *Critical Reviews in Biomedical Engineering*, 28, 2000, 75-80.
- [7] N. B. Wood, S. J. Weston, P. J. Kilner, A. D. Gosman and D. N. Firmin, Combined MR imaging and CFD simulation in the human descending aorta, *Journal of Magnetic Resonance Imaging*, 13, 2001, 699-713.
- [8] D. Lee and J. Y. Chen., Numerical simulation of steady flow fields in a model of abdominal aorta with its peripheral branches, *Journal of Biomechanics*, 35, 2002, 1115-1122.
- [9] Y. Tokuda, M. H. Song, Y. Ueda, A. Usui, T. Akita, S. Yoneyama and S. Maruyama, S., Three-dimensional numerical simulation of blood flow in the aortic arch during cardiopulmonary bypass, *European Journal of Cardio-Thoracic Surgery*, 33, 2008, 164-167.
- [10] M. Minakawa, I. Fukuda, T. Inamura, H. Yanaoka, K. Fukui, K. Daitoku, Y. Suzuki and Y. Hashimoto, Hydrodynamic evaluation of axillary artery perfusion for normal and diseased aorta, *General Thoracic and Cardiovascular Surgery*, 56, 2008, 215-221.
- [11] A. Assmann, A. C. Benim, A. Nahavandi, E. Turan, D. Schubert, E. Gams and P. Feindt, Aortic blood flow characteristics of different extracorporeal circulation techniques during cardiac surgery - a computational fluid dynamics approach, *IFMBE Proceedings 25/IV*, Springer, Berlin, 2009, 1604-1607.
- [12] <http://dicom.nema.org>.
- [13] S. Vikal, P. U. Thainual, J. A. Carrino, I. G. Iordachita, G. S. Fischer and G. Fichtinger, Perk station – percutaneous surgery training and performance measurement station, *Computerized Medical Imaging and Graphics*, Available online, doi: 10.1016/j.compmedimag.2009-05.001, 2009.
- [14] X. Papademetris, M. Jackowski, N. Rajeevan, R. T. Constable and L. H. Staib, *Bioimage Suite User's Manual*, [www.bioimagesuite.org](http://www.bioimagesuite.org) , 2008.
- [15] Ansys Fluent 12.0, *User's Guide*, Fluent Inc., Lebanon, NH, USA , 2009.
- [16] P. Khorrami, Numerische Analyse der Blutströmung im menschlichen Körper, M.Sc. Thesis, Duesseldorf University of Applied Sciences, Germany, 2009.
- [17] T. J. Pedley, Arterial and venous fluid dynamics, in: Pedrizetti G., and Perktold K. (Eds.) *Cardiovascular Fluid Dynamics*, Springer, Wien, 2003, pp 73-136.
- [18] F. R. Menter, Zonal two equation k-w turbulence models for aerodynamic flows, *AIAA Paper 93-2906*, 1993.
- [19] R. Peyret, *Handbook of Computational Fluid Mechanics*, Academic Press, San Diego, 1996.
- [20] F. N. van de Vosse, *Numerical Analysis of Carotid Artery Flow*, Dissertation, Technical University of Eindhoven, 1987.
- [21] S. Middleman, *Transport Phenomena in Cardiovascular System*, John Wiley & Sons, 1972.
- [22] A. C. Benim, A. Nahavandi, A. Assmann, D. Schubert, P. Feindt and S. H. Suh, Simulation of flow in human aorta with emphasis on outlet boundary conditions, *Applied Mathematical Modelling*, Appl Math Modell 2011; 35(7): 3175-3188. doi: 10.1016/j.apm.2010.12.022.
- [23] A. C. Benim, F. Gul, A. Nahavandi, A. Assmann, P. Feindt and F. Joos, Simulation of blood flow in human aorta for extracorporeal circulation, *Proc. 7th Int. Conf. Heat Transfer, Fluid Mechanics and Thermodynamics*, 19-21 July, 2010, Antalya, Turkey, 259-264.